Chemical Engineering Journal 200-202 (2012) 1–9

Contents lists available at SciVerse ScienceDirect

Chemical Engineering Journal

journal homepage: www.elsevier.com/locate/cej

Combustion synthesis of porous ZnO monoliths for sulfur removal

I. Perraud [a], R.M. Ayral [a,*], F. Rouessac [a], A. Ayral [b]

[a] Institut Charles Gerhardt, cc1504, C2M, Université Montpellier 2, Place E. Bataillon, 34095 Montpellier cedex 5, France
[b] Institut Européen des Membranes, cc047, Université Montpellier 2, Place E. Bataillon, 34095 Montpellier cedex 5, France

HIGHLIGHTS

- Simple and robust synthesis route for foam-like ZnO monoliths.
- Control of the monolith porosity thanks to the control of the combustion synthesis.
- Crystalline structure, microstructure and morphology characterization of the produced monoliths.
- Study of the monolith evolution after sulfidation–regeneration cycles.
- Applicability to sulfur removal.

ARTICLE INFO

Article history:
Received 28 March 2012
Received in revised form 31 May 2012
Accepted 5 June 2012
Available online 15 June 2012

Keywords:
Porous ZnO monolith
Combustion synthesis
Sulfur removal
Regenerable adsorbent

ABSTRACT

Highly porous ZnO monoliths are prepared with potential applications as regenerable adsorbents for sulfur removal. ZnS/NaCl composite materials are first obtained by combustion synthesis from mixtures of zinc, sulfur and sodium chloride powders. After NaCl removal by lixiviation with water, they are converted into ZnO by thermal treatment under air. The crystalline structure, the microstructure and the porosity of the resulting monoliths are investigated by X-ray diffraction, scanning electron microscopy and Hg porosimetry. Their evolution after sulfidation–regeneration cycles is also considered.

1. Introduction

Sulfur compounds, particularly H_2S, are severe poisons for metal catalysts used in chemical plants producing ammonia, methanol or hydrogen [1]. The reaction of sulfur compounds, particularly hydrogen sulfide, with metal oxides is of interest in connection with developing regenerable oxide sorbents for hot coal gas desulfurization [2,3]. Low-cost materials with high adsorption capacity like iron oxides are not convenient for desulfurization of feed gas in steam reformers. Zinc oxide enables to capture H_2S from reformate before it enters the water–gas-shift reactors to form ZnS and H_2O [4–10]. As the hydrocarbon feed passes through the catalyst bed, hydrogen sulfide is reversibly adsorbed by the active zinc oxide particles. Fixed beds of zinc oxide extrudates are currently used in production units. However, high capacity and regenerable monoliths would be a very attractive alternative. Such concept of adsorptive monoliths has been already considered in the past for designing rotating reactors enabling continuous regenerative H_2S removal [11].

This study deals with the development of a simple and robust synthesis route for foam-like ZnO monoliths applicable to sulfur removal. Several methods exist for the production of solid foams [12]. Here, we investigate the possibility of controlling size porosity in ZnO samples thanks to combustion synthesis or SHS (Self propagating High temperature Synthesis) [13]. This method involves exothermic reaction between solids, liquids, liquids/solids or gas/solids. The process can be divided in two stages, the initiation of the reaction and then, depending on experimental conditions, the propagation of combustion wave along a compact. This gives rise in a very short time to the total conversion of reactants into products. It is acknowledged that the combustion synthesis method has many potential advantages such as low processing cost, high energy efficiency, and high production rate [14,15].

Due to a very high exothermicity, the direct SHS of ZnO-based materials from Zn and O_2 does not allow the porosity control and the shape of the final product as the reaction is too explosive ($\Delta_f H_{ZnO} = -348$ kJ mol^{-1}). Some studies describe combustion synthesis of ZnO using glycine and zinc nitrate as reactants that

* Corresponding author.
E-mail address: rose-marie.ayral@univ-montp2.fr (R.M. Ayral).

1385-8947/$ - see front matter © 2012 Elsevier B.V. All rights reserved.
http://dx.doi.org/10.1016/j.cej.2012.06.010

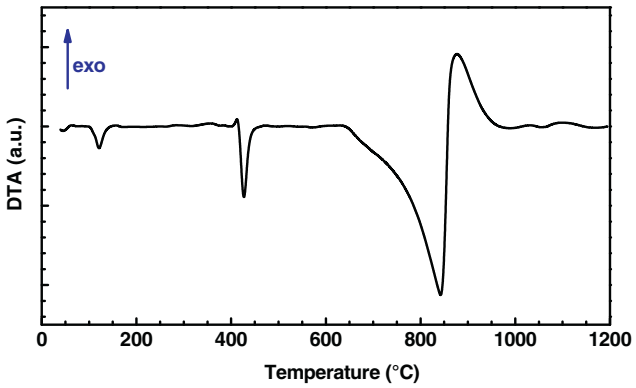

Fig. 1a. DTA curve for a Zn + S mixture.

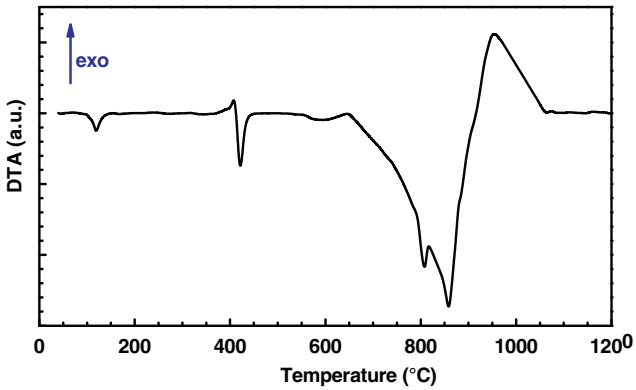

Fig. 1b. DTA curve for a Zn + S + NaCl-15 mixture.

leads to ZnO powders with controlled morphology [16,17]. Other study mentions Zn and NH_4NO_3 as reactants [18].

In this work, another synthesis approach is developed by preparing first ZnS monoliths from compacts of Zn and S powder mixtures ($\Delta_f H_{ZnS} = -189\ kJ\ mol^{-1}$) and converting them into ZnO thanks to a thermal post-treatment under air. This synthesis strategy has been already described by authors [13].

The propagation of the combustion wave determines the nature of the obtained material. In the case of explosive exothermic reaction, the initiation takes place simultaneously in each part of the sample, the initial compact shape is lost and control of porosity is not possible. Moreover, if the propagation is unstable, i.e. the rate of propagation of the combustion wave is not constant, combustion is of spin-type and the product reveals macroscopic heterogeneities [14]. With optimized experimental conditions, the combustion wave propagates along the sample. The propagation is stable when the combustion front is plane and this leads to homogeneous material. These different modes are governed by the exchange of heat between the compact and the surroundings. So, thermal conductivity is the most important parameter in the optimization of the process. Others key-parameters for optimizing the process are, the grain size of the powders constituting the green pellet, the compaction pressure, the gas pressure in the combustion chamber, the heating rate and the diluent amount in the reacting mixture [19]. Recent studies demonstrated that combustion synthesis can be used to form porous materials [20,21].

The first part of this paper describes the reaction between zinc and sulfur under argon pressure in order to define the type of combustion and to control it. NaCl salt is well known to be a porogen in ceramics [22–26]. It can be easily removable from the samples by lixiviation with water. ZnS/NaCl composite materials were then prepared by combustion synthesis from mixtures of zinc, sulfur and sodium chloride powders. The crystalline structure, the microstructure and the porosity of the resulting porous ZnO monoliths were investigated by X-ray diffraction, scanning electron microscopy and Hg porosimetry. Their evolution after successive cycles of sulfidation under H_2S and regeneration under air will be finally discussed.

2. Materials and methods

The starting powders were zinc (99.99% pure, mean particle size: 7.5 μm, Alfa Aesar Johnson Matthey), sulfur (reagent grade, mean particle size: 149 μm, Sigma Aldrich), and sodium chloride (99.5%, Prolabo sieved <50 μm) used as both diluent and porogen. The Zn/S molar ratio was fixed at 1:1. Different weight percentages of NaCl were tested considering the overall mixture Zn + S + NaCl: 5, 10, 15, and 20 (later labeled Zn + S + NaCl-*x*, where *x* is the value of NaCl weight percentage). The three powders have been mixed together in a Si_3N_4 jar without balls under argon for 12 h. The device used was a planetary mill (Fristch Pulverisette P7) operating at 490 rpm. Due to the absence of balls inside the bowl, only intimate mixing of Zn and S powders was obtained. No mechanical activation of these powders and no effect on ignition of the reaction were evidenced. The powder mixtures were uniaxially pressed into pellets of 13 mm or 22 mm in diameter in a floating die at a compaction pressure of 300 MPa. Preliminary experiments showed that no compaction effect was evidenced in the structure of final materials [13].

The combustion reactions were carried out in a conventional system SHS reactor under argon (gas pressure ranging from 0.2 MPa to 1.5 MPa). The device was composed of a steel cylindrical

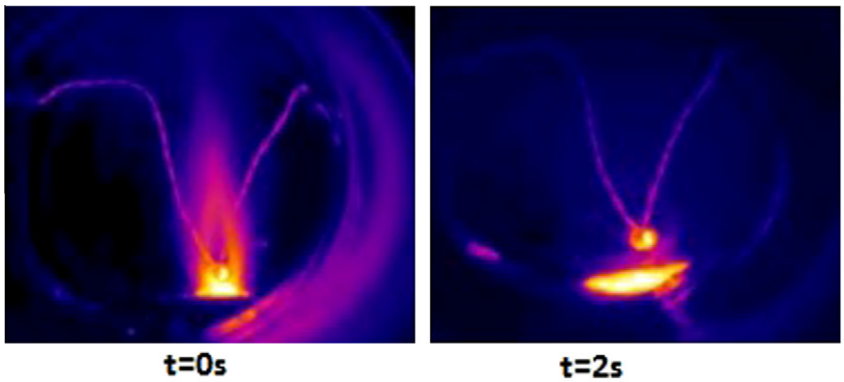

Fig. 2. Infra-red pictures of Zn + S reaction registered during combustion.

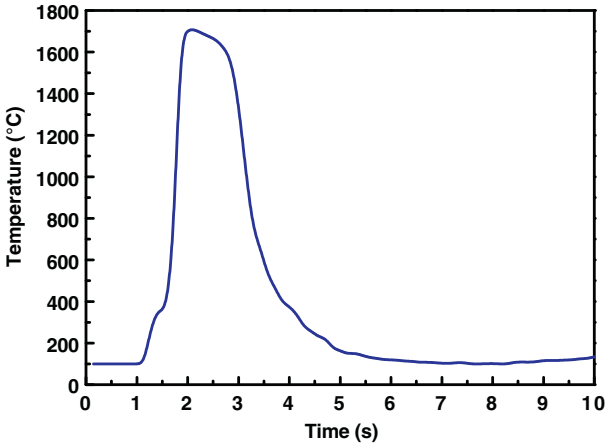

Fig. 3. Thermal profile registered during combustion synthesis of a Zn + S mixture.

reactor whose volume is 1 L. The pressure inside this reactor must not exceed 7 MPa and the temperatures of the walls cannot be higher than 50 °C. The overheating problem is prevented by a water cooling system. The lower part of the device consists of removal ceramic support made from pyrophyllite. After sample introduction, the reactor was closed, evacuated and filled with argon to the desired pressure. Ignition was provided by a tungsten filament positioned above the upper surface of the sample and was programmed to produce a voltage pulse of 50 V for 1–2 s. The power supply to the coil automatically stops after sample ignition.

In order to study the temperature evolution during combustion synthesis, two types of temperature measurements were used. Tungsten–Rhenium thermocouples (W/Re3 and W/Re25) were positioned in the upper and down side of the sample. The output signals of thermocouples (3 measurements per second) were acquired by a data acquisition card " Hi-speed USB Carrier National Instruments", with Labview software. In addition, the temperature evolution was followed by an IR video camera (FLIR A320 – spectral range [7.5–13 μm]) connected to ThermaCAM Researcher software. The camera allows spatial resolution of 1.36 mrd and an acquisition of 7 frames/s with a measurement range between 300 °C and 2000 °C. It was placed outside the reactor (room temperature) equipped with ZnSe windows (transparent to IR in the range of temperatures used during our synthesis). In order to quantitatively use the signal of the IR camera during the synthesis of zinc sulfide materials, we first need to estimate the emissivity of these materials. For this purpose, we measured the surface temper-

Table 1
Sample characteristics related to the SHS process.

Sample	Zn + S	Zn + S + NaCl-5	Zn + S + NaCl-10	Zn + S + NaCl-20
Initial diameter of pellet (mm)	13	13	22	22
Propagation rate (mm s^{-1})	Thermal explosion	0.9	2	Not measured
Volume expansion after SHS (%)	Shrinkage	~75	~25	~20
Compact morphology after SHS	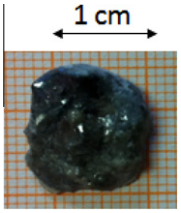	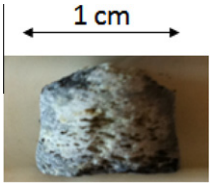	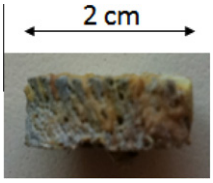	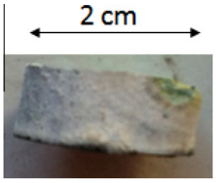

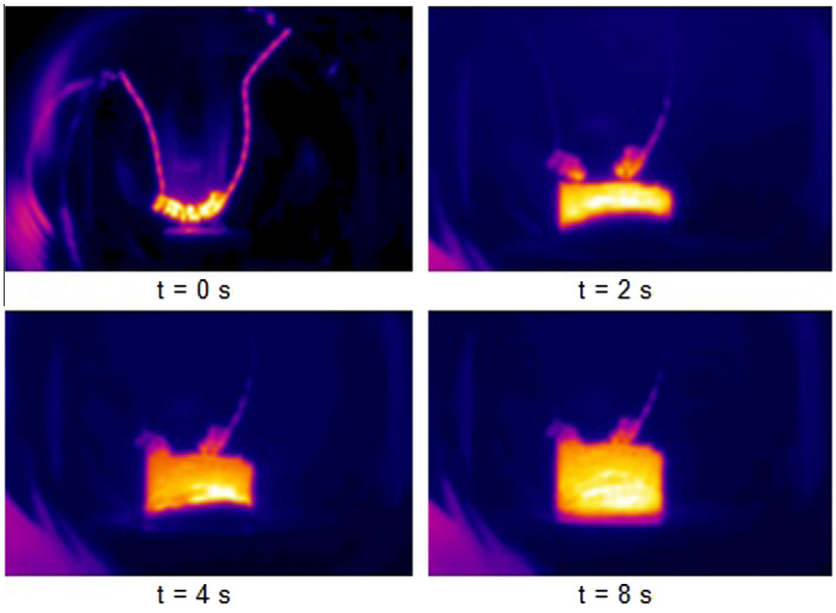

Fig. 4. Infra-red pictures recorded during combustion of a Zn + S + NaCl-5 compact.

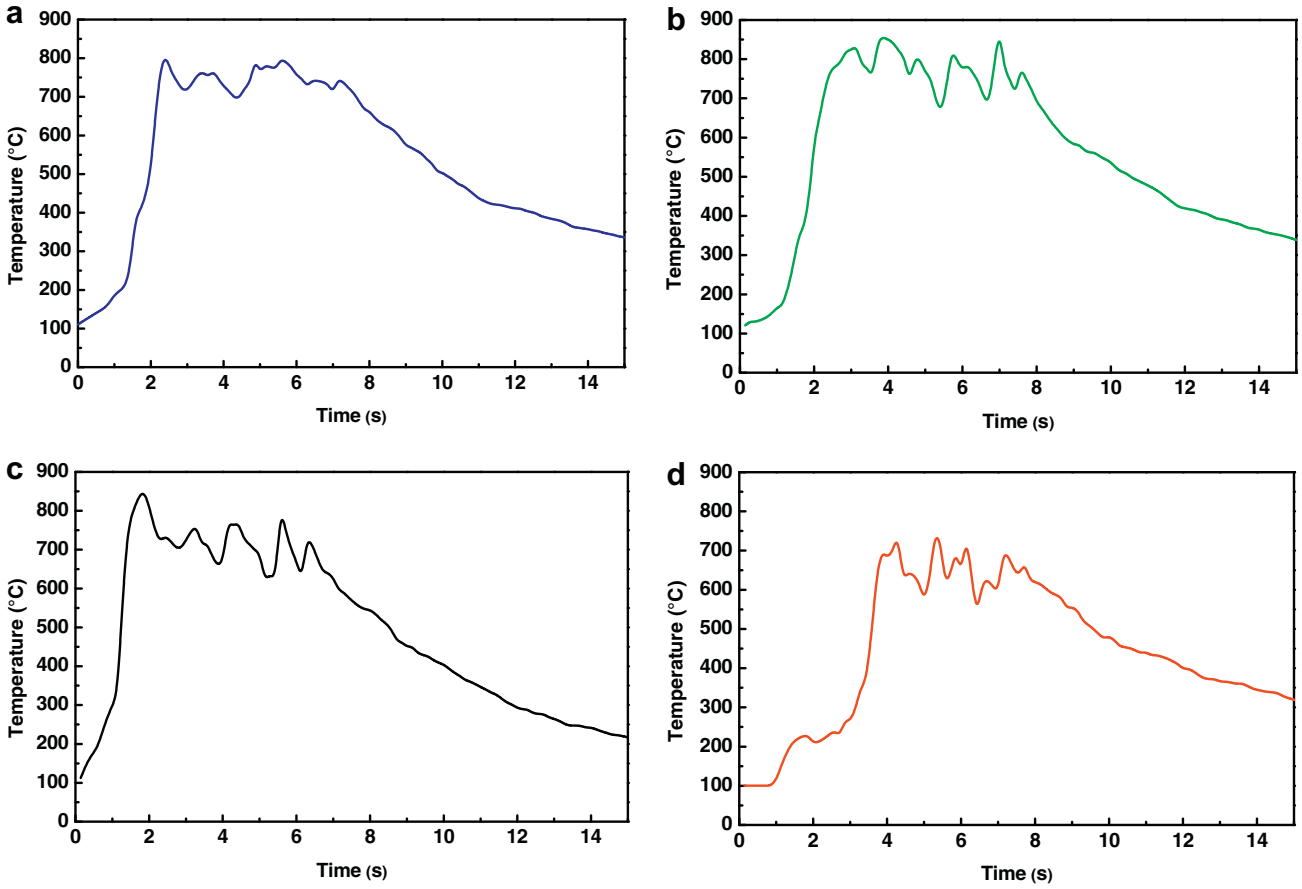

Fig. 5. Thermal profiles registered during combustion synthesis of (a) Zn + S + NaCl-5, (b) Zn + S + NaCl-10, (c) Zn + S + NaCl-15 and (d) Zn + S + NaCl-20 compacts.

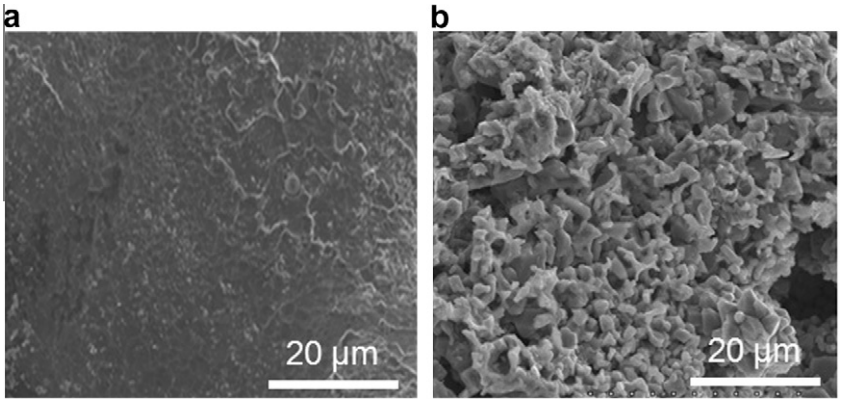

Fig. 6. SEM micrograph of (a) ZnS product (b) a fracture for a Zn + S + NaCl-20 monolith after combustion and NaCl removal.

ature of the material with thermocouple providing a reference temperature. In parallel, an image of the same surface was recorded using the IR camera. The thermal profile provided by the camera software was then fitted with the measurements from the thermocouples. The emissivity ε of the compact during combustion was then calculated by the camera software. The resulting value of ε in the spectral range [7.5–13 μm] is equal to 0.7.

After combustion synthesis, the resulting monoliths were immersed in water for NaCl removal. The conversion into zinc oxide was carried under air by heating the samples up to 800 °C during 2 h (heating rate of 5 °C min^{-1}).

For testing the ability of the ZnO samples to capture H_2S, the following reaction was studied:

$$ZnO(s) + H_2S(g) \rightarrow ZnS(s) + H_2O(g) \quad (1)$$

The thermal treatment for sulfidation consists of heating the sample up to 400 °C under pure N_2 flow. H_2S was produced by means of the following reaction:

$$FeS(s) + 2HCl \rightarrow H_2S(g) + FeCl_2(s) \quad (2)$$

It was then diluted in the nitrogen flow during the plateau at 400 °C during 4 h. The time of contact with H_2S was fixed in order to avoid a total conversion into ZnO. Cooling to room temperature was carried out in pure nitrogen atmosphere. Regeneration into ZnO was done applying the same conditions as for the initial conversion from ZnS.

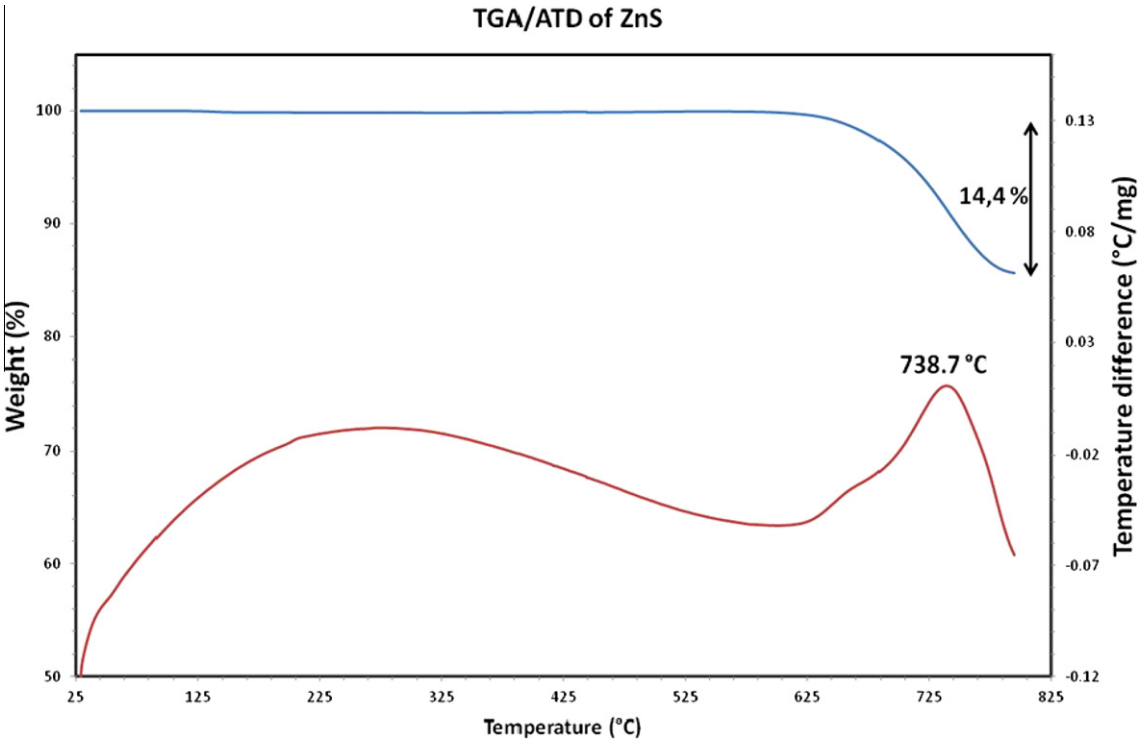

Fig. 7. TGA–ATD curve under O_2 flow for a powder from a Zn + S + NaCl-20 sample after lixiviation.

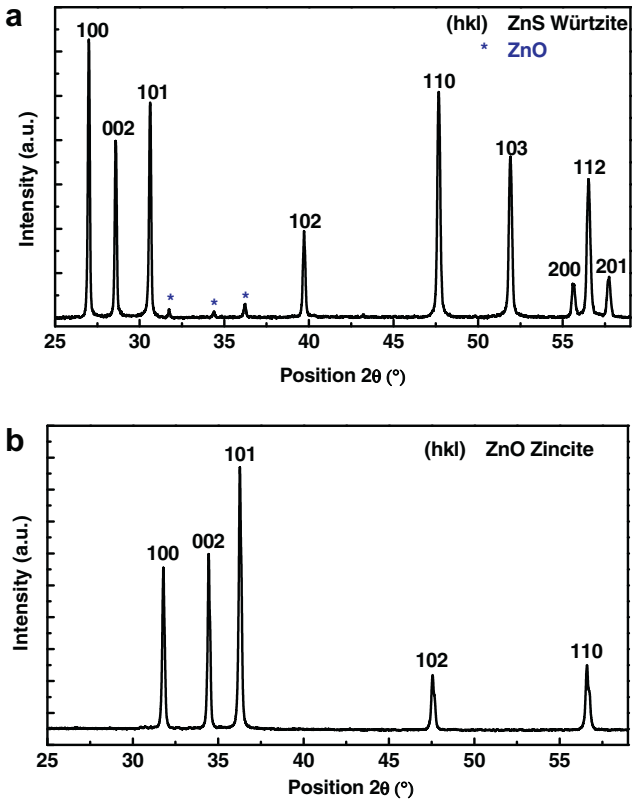

Fig. 8. X-ray diffractograms from a Zn + S + NaCl-20 sample before (a) and after thermal conversion into ZnO.

In addition, differential thermal analyses (DTA) of reacting mixtures were performed using Netzsch DSC 404 c Pegasus apparatus, under argon flow, with a heating rate of 5 °C min^{-1}. Thermogravimetric analyses (TGA) coupled with DTA were also performed on ZnS samples using SDT 2920 (TA Instruments), under air flow, with a heating rate of 5 °C min^{-1}.

The crystalline structure of combustion products and of ZnO samples was analyzed by X-ray diffraction (XPert pro, Cu Kα radiation) on powders prepared by grinding the samples in an agate mortar. Rietveld treatment of the diffractograms was done using the Fullprof software. The morphology of fracture surfaces was observed with a scanning electron microscope (SEM, Hitachi S-2600N). Pore volume and pore size distribution were analyzed by Hg porosimetry using a Micromeritics Autopore IV 9500 apparatus.

3. Results and discussion

3.1. Preliminary investigations on ignition phenomenon

In order to better understand the ignition mechanisms for combustion synthesis between Zn and S powders, in the absence or presence of NaCl, the thermal behavior of the various mixtures was preliminary studied by DTA. The DTA curve reported in Fig. 1a is related to a Zn + S mixture. It shows three endotherms and one exotherm. The first endotherms located at 120 °C and 420 °C correspond to the melting of S and Zn powders, respectively. Sublimation of melted sulfur started at 560 °C. Then the exotherm observed at 950 °C can be assigned to combustion reaction between zinc and sulfur. The DTA curve for a Zn + S + NaCl-15 mixture is given in Fig. 1b. In this case, an extra endotherm is observed corresponding to NaCl melting (801 °C). It shows that melting of NaCl joined to sublimation of sulfur give rise to ignition of the combustion reaction between zinc and sulfur. Moreover, these DTA experiments evidence that it is necessary to avoid sublimation of sulfur during combustion synthesis. It is why we chose to work under argon pressure in the reactor. All the experiments were conducted under 1.5 MPa of argon.

Table 2
Porosity of the different monoliths after conversion into ZnO.

Samples	Calculated porosity in the initial Zn + S + NaCl compact (%)	Calculated porosity in ZnO monolith (assuming no size change for the pellet) (%)	Measured porosity in ZnO monolith (±2%)	Average pore size in volume (μm)	Morphology (starting from pellets with an initial diameter of 22 mm)
Zn + S + NaCl-5	21	25	64	14	Too brittle
Zn + S + NaCl-10	14	24	60	16	
Zn + S + NaCl-15	11	21	64	17	
Zn + S + NaCl-20	11	22	71	12	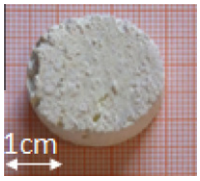

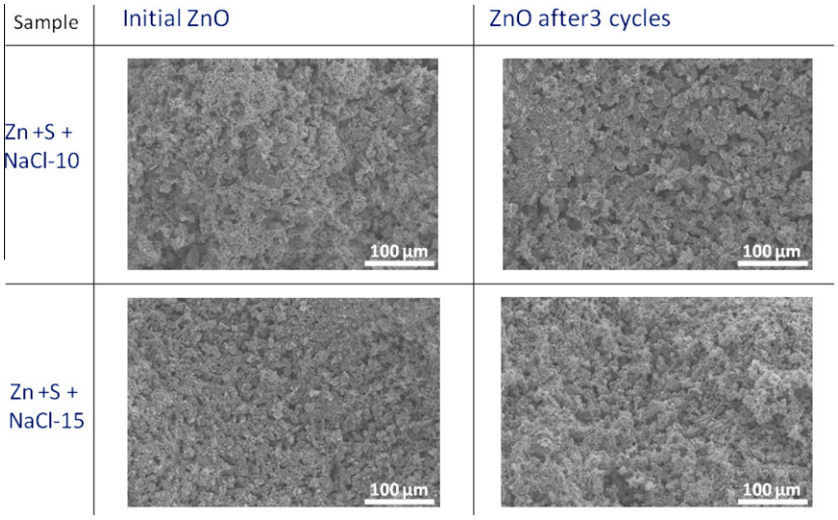

Fig. 9. SEM micrographs for ZnO monoliths.

3.2. Combustion synthesis

3.2.1. Study of Zn + S compacts

Fig. 2 shows a series of recorded images illustrating the combustion of a Zn + S compact. After ignition by the tungsten wire (t = 0 s), a thermal explosion occurs in the entire pellet giving rise to vapors of ZnS product evidenced by the presence of a halo on the recorded images (see t = 0 s) and by the presence of a ZnS deposits on the reactor walls after the experiment. The combustion is complete after 6 s.

In addition to the burning images, thanks to the integrated software of the camera, it is possible to get the evolution of temperature at the surface of the sample during the combustion (Fig. 3). The temperature increases very quickly to a maximum combustion temperature of 1620 °C and the reaction is very fast. The exothermic phenomenon only takes 3 s and the decreasing of temperature from maximum (1620 °C) to room temperature is very fast, about 1 s. Shrinkage and shape distortion were clearly observed for all the undiluted samples (Table 1).

3.2.2. Study of Zn + S + NaCl compacts

NaCl acts as a diluent. It decreases the combustion temperature and, by way of consequence, limits the densification and the shape distortion of pellets. Fig. 4 shows a series of recorded images illustrating the combustion of a Zn + S + NaCl-5 compact. After ignition, it is possible to follow the propagation of the combustion wave along the compacted sample. The exothermic phenomenon from ignition to end of propagation of the reaction along the compact

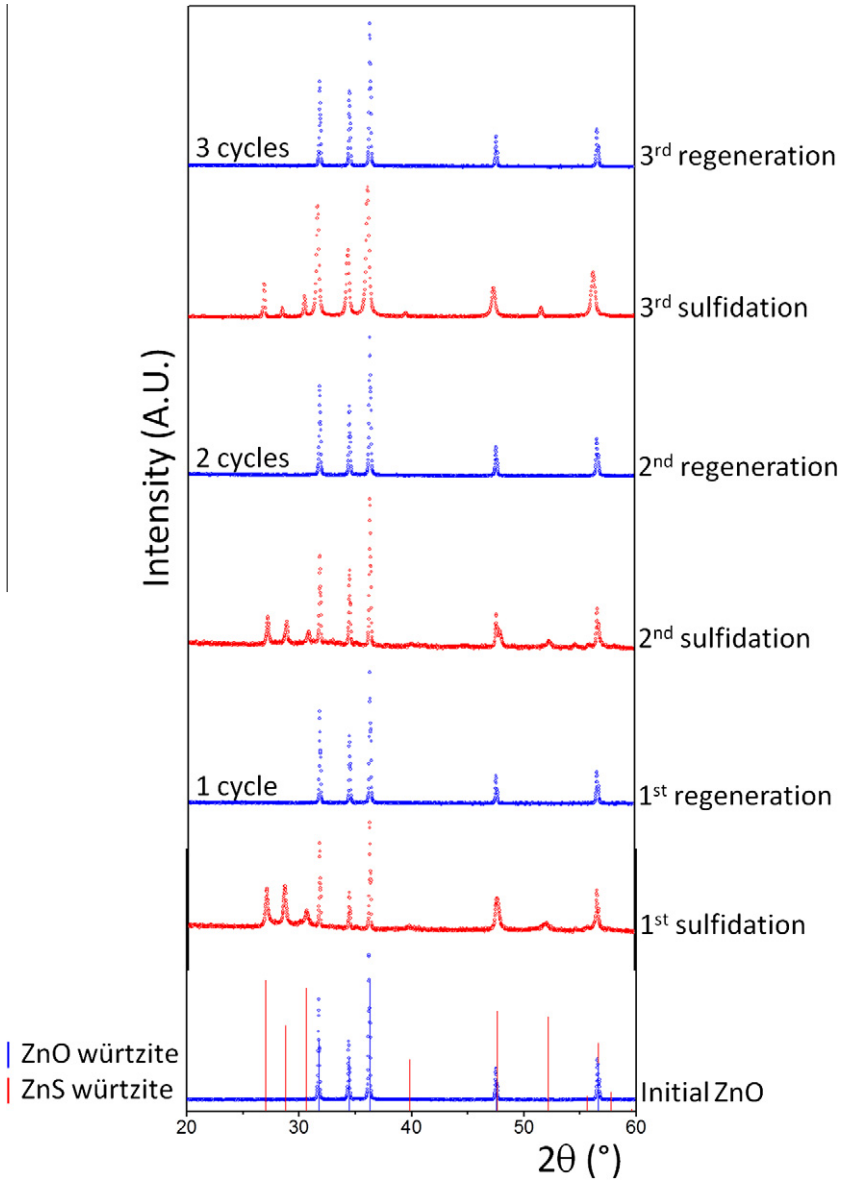

Fig. 10. X-ray diffractograms after each step of sulfidation and regeneration for a sample Zn + S + NaCl-10.

Table 3
Proportion of ZnO/ZnS in samples obtained after sulfidation.

	1st Sulfidation	2nd Sulfidation	3rd Sulfidation
Molar ratio ZnO/ZnS	80/20 ± 2%	90/10 ± 2%	85/15–2%

takes 8 s and is longer than previous sample. The temperature profile extracted from the IR camera signal is presented in Fig. 5a. Similar types of profiles were obtained for all the other tested mixtures containing NaCl Fig. 5b–d. Compared to mixtures without NaCl (Fig. 3), attenuation of the combustion process clearly occurs.

The temperature profile shows a rapid increase of temperature to 827 °C in the initial portion of the reaction zone. A long tail of the after-burning zone or zone-plateau then follows. This zone is constituted of thermal fluctuations with amplitude of ∼100 °C. During combustion, NaCl is melted and the temperature plateau corresponds to melting point of NaCl (801 °C). NaCl melting limits the exothermicity of the reaction between Zn and S. The thermal fluctuations observed correspond to a succession of endotherms and exotherms. The endotherms are due to the propagation of the wave through NaCl. We can define this phenomenon as pulsating combustion [27]. In such type of combustion, the combustion wave travels in a planar but pulsating manner which frequently results in materials with a laminated structure as experimentally observed (Table 1) [27]. This profile shows the influence of NaCl content on the combustion parameters. NaCl melting creates heat sinks in the sample. The heat release per unit volume and the maximum combustion temperature decrease whereas the wave velocity increases (Table 1). This propagation rate was determined by measuring, from the camera records, the time required by the propagation front to move between two points of the compact separated by a given distance. The lowest combustion temperature was obtained with a Zn + S + NaCl-20 compact. No more combustion can be detected when more than 30 wt.% of NaCl is added in the mixture.

Due to immiscibility between ZnS and NaCl, phase separation is preserved during the combustion process. A continuous network of ZnS is formed and liquid NaCl present at the propagation front is

Table 4
Porosity and average pore size in volume for ZnO monoliths.

Sample	Initial ZnO		ZnO after 1 cycle		ZnO after 2 cycles		ZnO after 3 cycles	
	Porosity (±2%)	Average pore size (μm)	Porosity (±2%)	Average pore size (μm)	Porosity (±2%)	Average pore size (μm)	Porosity (±2%)	Average pore size (μm)
Zn + S + NaCl-10	61	16	65	15	62	6	60	**7**
Zn + S + NaCl-15	65	17	70	14	68	7	68	**7**

segregated into the pore network. NaCl is then easily eliminated by lixiviation with water.

3.3. Morphology of the combustion products

Table 1 shows the reported experimental data about four samples prepared by combustion synthesis from compacts with different NaCl contents. The propagation rate of the combustion wave and the sample expansion after combustion are given. A picture of each sample is also included. It appears that the samples with the highest NaCl contents (10 and 20 wt.%) are not significantly deformed.

By SEM, the samples synthesized without NaCl appear with a dense microstructure resulting from high combustion temperature and melting of the product (Fig. 6a). When NaCl is added, a homogeneous and porous microstructure is observed after lixiviation (Fig. 6b).

3.4. Conversion of ZnS into ZnO

In order to optimize the conversion treatment from ZnS to ZnO, we performed thermogravimetric analyses coupled with a differential thermal analyses under air flow. Fig. 7 shows the resulting curves for a powder obtained by grinding a monolith Zn + S + NaCl-20 after lixiviation. It can be seen that the conversion proceeds in between 577 °C and 770 °C. The DTA curve exhibits an exotherm at 738 °C assigned to the conversion reaction. The weight loss determined from the TG curve is about 15% which agrees with the change from ZnS to ZnO (M_{ZnS} = 97 g mol^{-1} and M_{ZnO} = 81 g mol^{-1}).

During the monolith thermal treatment, sulfur dioxide generated by the reaction was extracted by the air flow maintained in the tubular furnace in order to avoid subsequent formation of zinc sulfate following reaction:

$$ZnO(s) + SO_2(g) + 1/2O_2(g) \rightarrow ZnSO_4(s) \quad (3)$$

Fig. 8a and b present the X-ray patterns from a Zn + S + NaCl-20 sample before and after thermal conversion. These patterns strictly correspond to that expected for ZnS würzite [28] and for ZnO zincite [29], respectively.

For application purpose, the treatment under air must not affect the mechanical integrity of the samples. This mechanical integrity is macroscopically confirmed for the tested compositions with an initial percentage of NaCl higher than 5% (Table 2) and will be kept after several regeneration cycles. Due to incomplete conversion of ZnO into ZnS, a continuous ZnO skeleton is preserved saving the monolith integrity. No significant macroscopic volume change is evidenced. Only pore volume is modified due to partial conversion of ZnO into ZnS and vice versa.

Taking into account the values of bulk density for the initial solid (ρ_{ZnS} würzite = 3.98 g cm^{-3}) and for the final solid (ρ_{ZnO} zincite = 5.61 g cm^{-3}) it is expected a volume decrease of solid phase equal to ~30% after conversion (expected linear shrinkage of ~10%). The size measurements performed on the monoliths before and after conversion enabled to estimate a linear shrinkage less than 1%. It can be deduced that the main part of the solid volume variation due to conversion generates additional porosity inside the monolith. Fig. 9 gives examples of microstructures observed by SEM after conversion into ZnO. Table 2 also summarizes the porosity and average pore size values measured by Hg porosimetry. The average pore size distribution is always very broad ranging from ~20 to ~0.1 μm with an average pore size in volume (corresponding to 50% of pore volume) located around 15 μm. The porosity values are also rather close, whatever the initial NaCl content, ranging from 60% to 70%. They can be usefully compared to the values calculated assuming no variation of the external dimensions of the starting compacts and porosity only associated with removal of the NaCl porogen phase and the ZnS–ZnO conversion. These calculated values (Table 2) are very low in comparison with the measured ones. This difference is easily explained by the sample expansion resulting from combustion synthesis. Added NaCl is clearly more crucial in term of diluent than of porogen. NaCl plays also a role in the shaping stage facilitating higher compaction rates due its plasticity (Table 2).

3.5. H_2S capture and adsorbent regeneration

Two samples, Zn + S + NaCl-10 and Zn + S + NaCl-15, were submitted to successive sulfidation–regeneration cycles.

Fig. 10 presents the diffractograms for the Zn + S + NaCl-10 after the different steps during 3 cycles. During each sulfidation stage, with the chosen experimental conditions, only one part of the ZnO phase is converted into ZnS. Rietveld analysis of these different diffractograms enabled us to estimate the molar percentages of the different phases after each of the three successive sulfidation steps (Table 3).

The microstructural evolution of the ZnO monoliths after sulfidation–regeneration cycles was studied. SEM images are shown in Fig. 9 and porosity data are reported in Table 4 for samples Zn + S + NaCl-10 and Zn + S + NaCl-15 after one, two and three regeneration cycles. Taking into account the accuracy of the measured values, it can be concluded that there is no significant change of total porosity. A small decrease of average pore size is observed during the first cycle (Table 4). This phenomenon can be assigned to the microstructure changes occurring at the pore surface. New population of small pores is created in the solid layers submitted to the cyclic conversions, with simultaneous reduction in size of the larger pores. The resulting effect is a shift of the average pore size to a smaller value.

The total porosity of the produced ZnO monoliths is ranging from 60% to 70% (Table 4). These values can be compared with those of packing of cylindrical extrudates in fixed beds. The average porosity between such packed cylinders is ranging from 30 to 40 [30] whereas the internal porosity of the commercial ZnO extrudates is usually ranging from 50% to 60%. The resulting total porosity for fixed beds can be estimated as ranging from 65% to 76%. The total porosity is quite the same for the two types of

adsorption devices and as the consequence their potential adsorption capacities per unit of volume are comparable.

4. Conclusion

Highly porous ZnO monoliths would be highly valuable materials as regenerable adsorbents for sulfur removal in industrial chemical processes. These preliminary results about the development of simple and robust preparation method using combustion synthesis demonstrate their feasibility of producing ZnO starting from compacts of zinc, sulfur and sodium chloride. Sodium chloride is added as both diluent and porogen, easily removable by lixiviation with water. The study reveals that its main effect is as diluent enabling to control the combustion process and to produce highly porous ZnO monoliths which can be regenerated after H_2S capture without significant change of porosity.

Efforts will be made in the next future for scaling up, in order to demonstrate that efficient gas contactors with adapted size and adsorption capacity can be obtained by extrapolating the current results.

Acknowledgments

The authors would like to thank Mathias Haacké (ICGM) for help in SHS experiments, A. El Mansouri (IEM) and D. Granier (ICGM) for Hg porosimetry and X-ray diffraction measurements, respectively.

References

[1] P.J.H. Carnell, in: M.V. Twigg (Ed.), Feedstock Purification in Catalyst handbook, second ed., Wolfe Publishing Ltd., London, 1989, pp. 191–224.
[2] J-C. Hoguet, G.P. Karagiannakis, J.A. Valla, Christos C. Agrafiotis, A.G. Konstandopoulosa, Gas and liquid phase fuels desulphurization for hydrogen production via reforming processes, Int. J. Hydrogen Energy 34 (2009) 4953–4962.
[3] S. Lew, A.F. Sarofim, M. Flytzani-Stephanopoulos, Modeling of the sulfidation of zinc-titanium oxide sorbents with hydrogen sulfide, AlChE J. 38 (1992) 1161–1169.
[4] S. Lew, K. Jothimurugesan, M. Flytzani-Stephanopoulos, High temperature H_2S removal from fuel gases by regenerable zinc-oxide- titanium dioxide sorbents, Ind. Eng. Chem. Res. 28 (1989) 535–541.
[5] J.M. Davidson, C.H. Lawrie, K. Sohail, Kinetics of the absorption of hydrogen sulfide by high purity and doped high surface area zinc oxide, Ind. Eng. Chem. Res. 34 (1995) 2981–2989.
[6] W.F. Elseviers, H. Verelst, Transition metal oxides for hot gas desulphurization, Fuel 78 (1999) 601–612.
[7] I.I. Novochinskii, C. Song, X. Ma, X. Liu, L. Shore, J. Lampert, R.J. Farrauto, Low-temperature H_2S removal from steam-containing gas mixtures with ZnO for fuel cell applications 1 ZnO particles and extrudates, Energ. Fuel 18 (2004) 576–583.
[8] L. Li, D.L. King, H_2S removal with ZnO during fuel processing for PEM fuel cell applications, Catal. Today 116 (2006) 537–541.
[9] K.H. Hassan, Regeneration and activity test of spent zinc oxide hydrogen sulfide removal catalyst, Eur. J. Sci. Res. 39 (2010) 289–295.
[10] N.-K. Park, G.-B. Han, S.-H. Yoon, S.-O. Ryu, T.-J. Lee, Preparation and absorption properties of ZnO nanostructures for cleanup of H_2S contained gas, Int. J. Prec. Eng. Manuf. 11 (2010) 321–325.
[11] W.J.W. Bakker, M. Vriesendorp, F. Kapteijn, J.A. Moulijn, Sorbent development for continuous regenerative H_2S removal in a rotating monolith reactor, Can. J. Chem. Eng. 74 (1996) 713–718.
[12] Y. Conde, J.F. Despois, R. Goodall, A. Marmottant, L. Salvo, C. San Marchi, A. Mortensen, Replication processing of highly porous materials, Adv. Eng. Mater. 8 (2006) 795–803.
[13] F. Rouessac, R.M. Ayral, A. Ayral, Preparation of ZnO filters via SHS of ZnS monoliths, Int. J. Self Prop. High Temp. Syn. 18 (2009) 283–286.
[14] A.S. Mukasyan, A.S. Rogachev, A. Varma, Mechanisms of reaction wave propagation during combustion synthesis of advanced materials, Chem. Eng. Sci. 54 (1999) 3357–3367.
[15] K. Morsi, The diversity of combustion synthesis processing: a review, J. Mater. Sci. 47 (2012) 68–92.
[16] C-S. Lin, C-C Hwang, W-H lee, W-Y Tong, Preparation of zinc oxide (ZnO) powders with different types of morphology by a combustion synthesis method, Mater. Sci. Eng. B 140 (2007) 31–37.
[17] C.-C. Hwang, T.-Y. Wu, Synthesis and characterization of nanocrystalline ZnO powders by a novel combustion synthesis method, Mater. Sci. Eng. B 111 (2004) 197–206.
[18] C-C. Hwang, C-S. Lin, G-P. Wang, C-H. Peng, S-L. Chung, A self-propagating high-temperature synthesis method for synthesis of zinc oxide powder, J. Alloy. Compd. 467 (2009) 514–523.
[19] M.C. Dumez, R.M. Marin-Ayral, J.C. Tedenac, The role of experimental parameters in combustion synthesis of NiAl under high gas pressure, J. Alloy. Compd. 268 (1998) 141–151.
[20] O.K. Kamynina, S.G. Vadchenko, A.E. Sytschev, A.S. Rogachev, L.M. Umarov, N.V. Sachkova, High porosity TiAl foam by volume combustion synthesis, Int. J. Self Prop. High Temp. Syn. 16 (2007) 137–140.
[21] S.G. Vadchenko, Formation of porous structure in SHS products, Int. J. Self Prop. High Temp. Syn. 19 (2010) 224–226.
[22] Y.Y. Zhao, D.X. Sun, A novel sintering-dissolution process for manufacturing Al foams, Scripta Mater. 44 (2001) 105–110.
[23] H.H. Nersisyan, J.H. Lee, C.W. Won, Combustion of TiO_2–Mg and TiO_2–Mg–C systems in the presence of NaCl to synthesize nanocrystalline Ti and TiC powders, Mater. Res. Bull. 38 (2003) 1135–1146.
[24] D.X. Sun, Y.Y. Zhao, Phase changes in sintering of Al/Mg/NaCl compacts for manufacturing Al foams by the sintering and dissolution process, Mater. Lett. 59 (2005) 6–10.
[25] H.H. Nersisyan, H.I. Won, C.W. Won, Combustion synthesis of WC powder in the presence of salts, Mater. Lett. 59 (2005) 3950–3954.
[26] H-Il. Won, H.H. Nersisyan, C.W. Won, A macrokinetic study of the WO_3/Zn reaction diluted with NaCl, Chem. Eng. J. 153 (2009) 193–198.
[27] S. Gennari, U. Anselmi-Tamburini, F. Maglia, G. Spinolo, Z.A. Munir, Simulation study of wave propagation instabilities for the combustion synthesis of transition metals aluminides, J. Phys. Chem. B 110 (2006) 7144–7152.
[28] S. Knitter, M. Binnewies, Chemical vapor transport of solid solution. Chemical transport of MnS/ZnS, FeS/ZnS, and FeS/MnS mixed crystals, Z. Anorg. Allg. Chem. 625 (1999) 1582–1588.
[29] S. Locmelis, M. Binnewies, Chemical vapor transport of solid solution. chemical transport of CuO/ZnO mixed crystals, Z. Anorg. Allg. Chem. 625 (1999) 1578–1581.
[30] W. Zhang, K.E. Thompson, A.H. Reed, L. Beenken, Relationship between packing structure and porosity in fixed beds of equilateral cylindrical particles, Chem. Eng. Sci. 61 (2006) 8060–8074.